J Therm Anal Calorim (2012) 109:1473–1479
DOI 10.1007/s10973-012-2212-y

Cu–ZnO nanocrystallites by aqueous thermolysis method

Thermal and vibrational study

Supriya N. Rishikeshi · Satyawati Joshi

Received: 13 June 2011 / Accepted: 13 January 2012 / Published online: 26 January 2012

Abstract ZnO and different atomic percentages of Cu-doped ZnO nanocrystallites have been prepared by aqueous thermolysis method using Glycine as a fuel and encapsulating agent. Mechanism and formation of intermediate products have been given for the first time. All the findings given are for samples annealed at 800 °C. XRD of nanocrystalline ZnO and Cu–ZnO has been indexed to hexagonal wurtzite structure. Influence of temperature on thermal properties of gel precursor and Cu-doped ZnO nanoparticles have been investigated using thermogravimetric and differential thermal analysis. Accordingly, samples have been annealed at different temperatures. Infrared studies revealed formation of Cu–ZnO nanoparticles and removal of organic matter at higher temperature.

Keywords Aqueous thermolysis · *Trans*-zinc glycinate complex · Thermal analysis

Introduction

Quantum dots of II–VI semiconductors are direct-bandgap materials and allow manipulation of properties by controlling the stoichiometry. ZnO is n-type semiconductor having wide and direct band gap of 3.37 eV with a large exciton binding energy of 60 meV, hence displays excellent piezoelectric and optical properties. It has been widely used as a low voltage phosphor [1], gas sensor [2], photocatalyst [3], and as varistors [4]. It is also used in paints and ceramics due to low coefficient of thermal expansion. It is used in cosmetic products, because of antifungal activity [5].

Various methods are available for synthesis of ZnO nanoparticles like sol–gel method [6], electrochemical [7], spray pyrolysis [8], thermal decomposition [9], wet chemical synthesis and combustion method [10–12], low pressure sputtering [13], oxalate route [14], etc. Among all these methods, aqueous thermolysis method is simpler and inexpensive. This is a quick and energy-efficient way to prepare valuable materials. Simple and mixed nano-oxides can be easily prepared by this method. In thermolysis, organic compound or polymer is used as a fuel [such as glycine, urea, citric acid, PVA, PVP] which is stoichiometrically added with metal nitrates, glycine (NH_2CH_2COOH) [15] is selected as a fuel since it is inexpensive, readily available, and its heat of combustion (−3.24 kcal/g) is more negative than urea and citric acid. Here, glycine also acts as capping agent to restrict the growth of ZnO and Cu-doped ZnO nanocrystals. In this reaction, metal nitrates play dual role, they act as metal source and as an oxidizer to promote the decomposition of metals and fuel (glycine). The method involves exothermic redox reaction of oxidizer (metal nitrates) and fuel, transition metal forms complex with the fuel during aging which slowly on heating evaporates water content and various gases forming nanosized oxides with carbonaceous matter of the fired fuel.

In our earlier papers, we have reported spherical- and cuboid-shaped ZnO nanoparticles and studied the role of polymer interactions during aqueous polymer thermolysis

Electronic supplementary material The online version of this article (doi:10.1007/s10973-012-2212-y) contains supplementary material, which is available to authorized users.

S. N. Rishikeshi · S. Joshi (✉)
Department of Chemistry, Center for Advanced Studies in Chemistry, University of Pune, Pune 411 007, India
e-mail: ssjoshi@chem.unipune.ac.in; ssjoshi@chem.unipune.ernet.in

[16]. Nanocubes of α-Fe_2O_3 were also prepared using polyvinyl alcohol of different molecular weights [17].

Doping has been widely used method to improve the various properties such as electrical, optical, and mechanical of semiconductor compounds, facilitating the construction of many electronic and optoelectronic devices. Cu-doped ZnO, is a p–n heterocontact system, CuO is a p-type semiconductor having narrow band gap between 1.21 and 1.5 eV. Cu shows properties as luminescent activator and as compensator for n-type semiconductors, ZnO is known to improve dispersion of copper and its reducibility. Cu functions as a catalyst in ZnO nanoparticle growth if incorporated as a dopant during synthesis, Cu–ZnO enhances antirust property [18]. Cu behaves as an acceptor in ZnO with its energy level locating at 0.17 eV below the bottom of the conduction band, making itself a good candidate for creating p-type ZnO [19]. Synthesis of Cu–ZnO has been reported earlier by solvated metal ion dispersion (SMAD) [20], plasma-assisted molecular beam epitaxy (PA-MBE) [21], Cu–ZnO nanosheets; synthesized recently using solution route [22], Cu–ZnO films have been prepared by sol–gel-derived dip-coating process [23], and magnetron sputtering [24], Cu–ZnO rods have been reported by hydrothermal method [25], nanonails and nanoneedles are also synthesized in one-end sealed slender quartz tube [26]. Highly sophisticated machinery and experimental setup has been used for synthesis of nanostructures. Herein, we report synthesis of Cu–ZnO by simple, easy, and inexpensive aqueous thermolysis method, using biocompatible amino acid.

Experimental procedure

Synthesis of undoped ZnO and Cu–ZnO

Synthesis of undoped ZnO and Cu-doped ZnO is as follows. Zinc nitrate hexahydrate [Zn $(NO_3)_2{\cdot}6H_2O$] Merck, Cupric nitrate trihydrate (Indian made CHD) [Cu $(NO_3)_2{\cdot}3H_2O$] AR grade, were used as Zn and Cu sources, respectively, and glycine (Thomas baker) as a fuel. Stoichiometric amounts of metal nitrates were mixed with glycine and 10% w/v of distilled water was added. In our opinion, it is appropriate to add 10% w/v distilled water. This precursor solution was aged for 2 h at room temperature and then slowly heated with manual stirring to form homogeneous polynuclear coordination precursor. An organic gel was formed, followed by decomposition of nitrates with evolution of brown fumes of nitrogen dioxide, which on further heating formed sticky paste, and then slowly turned into dry black fluffy powder. The results which are shown are only for samples annealed at 800 °C.

Sample characterizations

X-ray powder diffraction (XRD) patterns for as prepared and calcined powders were recorded using Philips PW 1840 powder X-ray diffractometer with Cu Kα radiation at room temperature. Transmission electron micrographs (TEM) were obtained on Philips CM 200. For this purpose, the powder was dispersed ultrasonically using ethanol. A drop of solution was placed on a carbon-coated copper grid and dried before analysis. To understand the functionality and composition of as prepared and annealed samples, infrared spectra were taken using FTIR 8400 spectrophotometer. Sampling was done with KBr pellet. The thermal decomposition pattern of the precursor and as prepared powder was studied by simultaneous differential thermal analysis (DTA) and thermogravimetric (TG) analysis on a STAR SW9.0. The TG–DTA analysis for all the samples was done from RT to 900 °C in dry air. The heating rate was maintained at 10 °C min^{-1}.

Results and discussion

Reaction mechanism

The nature and structure of glycine and its affinity toward solvent seem to be responsible for the formation of ZnO and its morphology. The interaction of amino acids and peptides with metal ions in solution has been extensively studied [27, 28]. Recently, we have studied structural phase behavior and vibrational spectroscopic studies of biofunctionalized CdS nanoparticles [29]. The mechanism behind combustion synthesis is initial formation of complex with glycine during aging (as shown in Scheme 1) where glycine acts as a bidentate ligand. Two molecules of glycine will bind with metal cation through carboxylate and amine group. With slow heating, water molecule will react with the complex, breaking Zn–N bond and C–C bond by nucleophilic attack forming zinc carbonate and methyl amine (NH_2–CH_3). These products on further heating will form ZnO (since decomposition temperature of zinc carbonate is $\sim$133 °C) followed by decomposition of methyl amine as CO_x and NO_x as shown in the schematic representation. There is also probability of formation of *trans*-copper glycinate complex depending on the concentration of copper as a dopant.

According to earlier research by Hwang et al. [15], it was found that nature of combustion characteristics of as prepared powders depend on glycine/nitrate ratio (G/N ratio). For fuel lean precursors, due to inadequate fuel concentration heat release is not enough to form well-developed phase of ZnO but in case of higher G:N mole ratio (4:1) oxygen contained in precursor is adequate and is

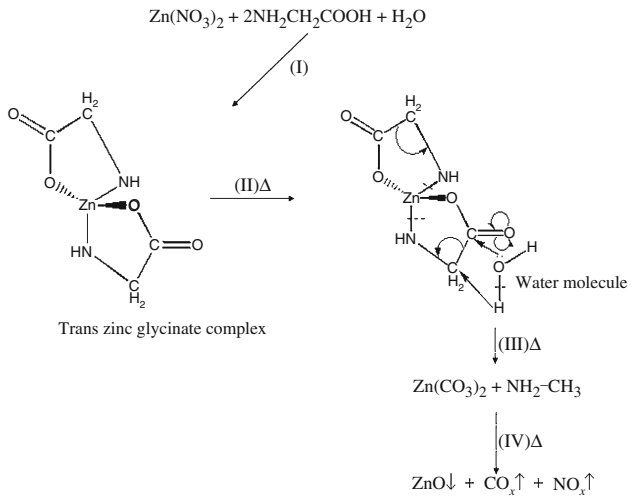

Scheme 1 Mechanism for formation of ZnO nanoparticles

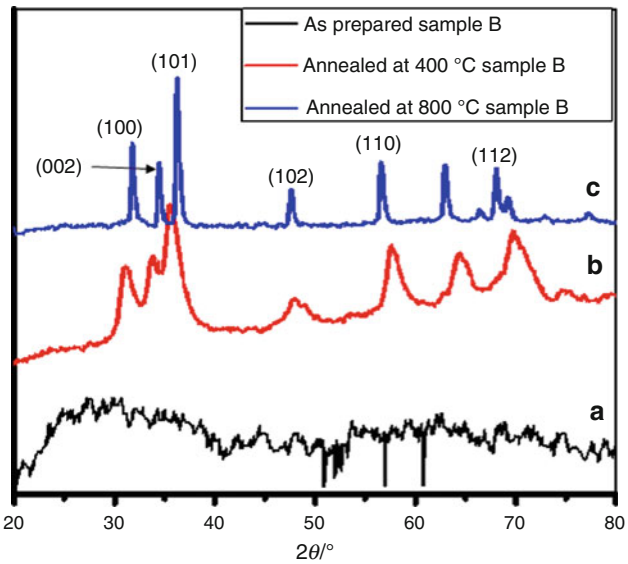

Fig. 1 XRD patterns of sample B: (*a*) as prepared, after annealing at (*b*) 400 °C and (*c*) 800 °C

the main source of oxygen required for combustion reaction. In fuel-rich ratio, total mole of gaseous products increases leading to disintegration of agglomerates, thereby hindering particle growth. It was observed that specific surface area for fuel-rich powder was larger as compared to fuel lean powder leading to lower particle size. Stoichiometry of the redox mixture is calculated based on total reducing and oxidizing valences of oxidizer (metal nitrates) and fuel (glycine) in the reaction and G/N ratio is maintained to 4 for all the undoped ZnO and various atomic percentages of Cu-doped ZnO powders. The synthesized products are hereafter designated as sample A—undoped ZnO, B–E are 0.1, 0.5, 1, and 5% Cu-doped ZnO, respectively.

According to earlier reports [15, 30], combustion was carried out without addition of water, only physical mixing of metal salts and fuel used to be done, but this method has certain limitations like inadequate water content, physical mixing of powders may lead to inhomogeneity, and high heat evolution by precursors and fuel, leading to larger grain size. Therefore, addition of 10% w/v water is necessary for homogeneous mixing and uniform smaller particle size.

X-ray diffraction analysis

The as prepared samples obtained by aqueous thermolysis method were characterized by XRD and are X-ray amorphous in nature. The X-ray diffractograms of 0.1% Cu-doped ZnO, as prepared and annealed at 400 and 800 °C are shown in Fig. 1. X-ray diffractograms of samples annealed at 400 and 800 °C show well-grown planes and accordingly crystallite size also increases with temperature following the diffusion mechanism. The average crystallite size was calculated from FWHM using Scherer formula for (100), (101), and (110) planes. Cluster sizes of samples annealed at 400 °C are 21(±1), 12(±1), 18(±1), 26(±1), 20(±1) nm for samples A–E, respectively. Accordingly, sample B shows minimum size at 400 °C. Sample E shows comparable sizes to sample A. While samples annealed at 800 °C are around 30–40 nm of size. The crystallite size was again confirmed from TEM image (shown in Fig. 2) of sample A annealed at 800 °C showing average particle size of 35 nm. All *d*-values of undoped and doped ZnO show hexagonal phase and wurtzite symmetry (JCPDS card no. 5-664). The broadening of peaks and slight difference in 2θ values for Cu-doped ZnO demonstrates the existence of minor strain in the crystal due to introduction of metal ion [31]. This strain in the crystal indicates incorporation of Cu^{2+} in the ZnO lattice via diffusion where it substitutes Zn^{2+} ions as ionic radius of Cu^{2+} (0.073 nm) is comparable than that of Zn^{2+} (0.074 nm). Samples are not showing any change in diffraction pattern at low doping (samples B and C) but at higher doping (samples D and E) extra reflections at 34.5° and 38.5° are observed (XRD patterns are not shown here). These results indicate that Cu has been doped into the ZnO lattice at lower doping and above 1% of copper doping CuO begins to form as an impurity.

FTIR analysis

FTIR spectra of undoped and Cu-doped ZnO samples and after annealing at 400 and 800 °C are obtained in the range of 350–4000 cm^{-1}. Figure S1 (given in the supporting material) shows FTIR spectrum of glycine. The percentage transmittance observed for glycine is comparable to those

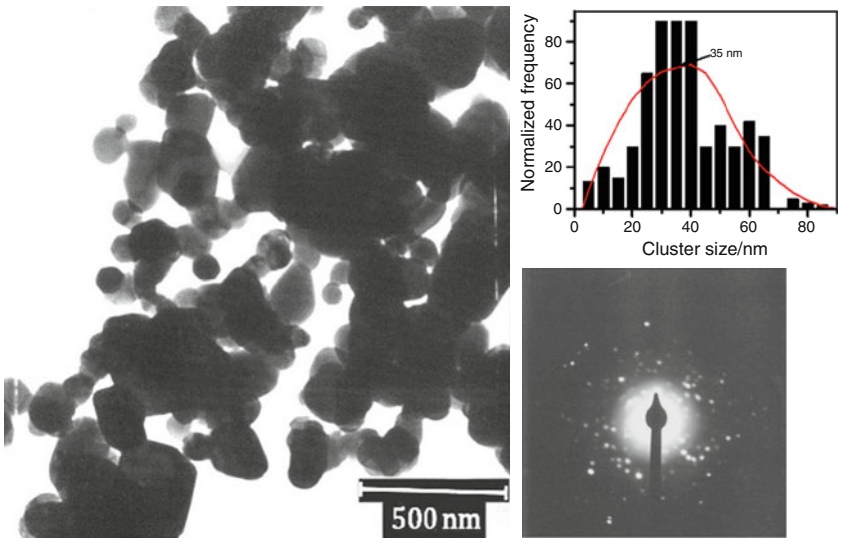

Fig. 2 TEM image and electron diffraction spot pattern of sample A, after annealing at 800 °C with corresponding size histogram *inset*. The *solid line* is a Gaussian fit to the data

reported earlier for pure zwitterionic glycine [32]. As shown in Fig. S1, a very broad band in the 2430–3420 cm^{-1} region indicates O–H stretching overlaps, it is also indicative of intermolecular hydrogen bonding between glycine molecules. NH_2 stretching frequency around 3260–3340 cm^{-1} and CH_2 symmetric and asymmetric stretching frequencies around 2899 and 2970 cm^{-1}, respectively, are observed in the broad absorption region along with wagging mode at 1332 cm^{-1} and scissoring mode at 1442 cm^{-1} for $–CH_2$. Absorption around 1606 cm^{-1} is NH_2 bending mode which is indicative of primary amine. Sharp bands at 1112 and 1132 cm^{-1} indicates NH_3^+ rocking mode. A sharp band at 1033 cm^{-1} shows C–C–N stretching mode [31, 33], while bands at 505 and 698 cm^{-1} show COO^- rocking and wagging modes, respectively. Absence of (C=O) stretching region at 1700–1800 cm^{-1} indicates that glycine is in zwitterionic state and reactive species is COO^- rather than (–COOH) acidic group [32].

The FTIR spectra taken for as prepared samples as well as after annealing at 400 and 800 °C are presented in Fig. 3 for sample A (FTIR spectra for samples B–E are given in supporting material as Fig. S2). All IR spectra of as prepared powders (A–E) show a broad band in the region 3300–3600 cm^{-1} which indicates N–H asymmetric stretching, this band can also be attributed to O–H stretching of physisorbed H_2O or from surface Zn–OH groups. Small bands at 2823 and 2910 cm^{-1} indicate CH_2 symmetric and asymmetric stretching frequencies of unreacted glycine. A small band at 823 cm^{-1} is assigned to C–H out of plane mode. Small bands around 870–980 cm^{-1} are observed after calcination which are assigned to hydrogen bonded O–H out of plane bending [34]. These bands almost vanish after annealing. Strong bands in the region 1200–1700 cm^{-1} with small shoulders are seen in all as prepared samples A–E and

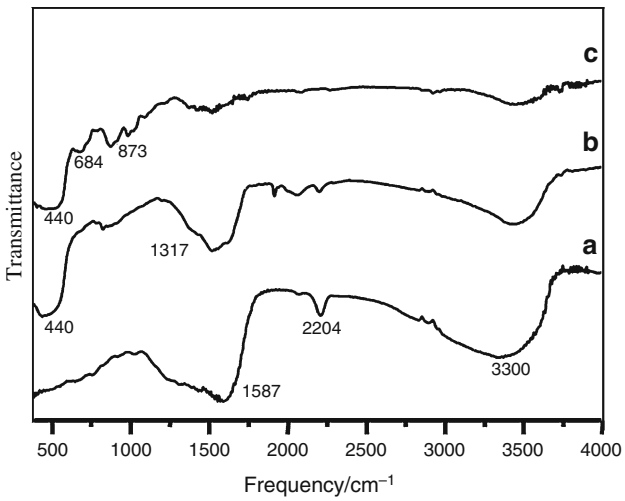

Fig. 3 IR spectra for sample A: (*a*) as prepared at (*b*) 400 °C and (*c*) 800 °C

assigned to carbonate species formed by coordination of CO_2 molecules onto coordinatively unsaturated ZnO surface, which is again confirmed by the proposed mechanism (Scheme 1). Similar type of formation of carbonates was observed in the preparation of other metal oxides by thermolysis using glycine [35, 36]. There is a band around 2204 cm^{-1} which is assigned to aliphatic cyanide group formed during complexation reaction with metal nitrates [32]. Glycine has two potential binding sites, amine and carboxylate group. The Zn–O stretching mode appears as a broad band around 440 cm^{-1} [16] shoulder band around 662 cm^{-1}; indicative of Cu–O stretching vibration. Cu–O stretching frequency around 481 cm^{-1} confirms the formation of Cu–O bond. The XRD peaks obtained at 34.5° and 38.7° for CuO are evidenced by FTIR frequencies at 662 and 481 cm^{-1}.

The solutions containing glycine are known to form metal glycino complexes, e.g., $Zn(NH_2CH_2COO)_2$ and $Cu(NH_2CH_2COO)_2$ where Cu^{2+} and Zn^{2+} ions react with two glycine molecules to give a chelate structure [33]. In such species, the glycine is present in its anionic glycinate form. Here, copper and zinc atoms are bound to one oxygen atom and the nitrogen atom of each glycinate species in the chelate structure.

With heating during synthesis, NH_3 evolution is confirmed by the disappearance of FTIR bands 3170 (υNH_2), 1516 (δ_{sim} NH_3^+), 1112 (ρrNH_3), 1033 ($\upsilon_{as}CCN$), and 893 ($\upsilon_{sim}CCN$) cm^{-1} in the as prepared products. Formation of condensation products of glycine might be responsible for this decomposition step, which also supports the decomposition steps in thermal study of precursor gels.

Thermal analysis

Influences of temperature on thermal properties are thoroughly studied by comparing TG–DTA curves of gel precursors and as prepared materials of the same sample and thereby we can monitor loss of carbonaceous matter and other gaseous products with temperature [37]. It is also necessary to understand the thermal decomposition of the gel before combustion and compare it to the decomposition of the pure glycine. Similar studies have been done by us on ZnO nanoparticles using PVA as an encapsulating agent and as a fuel [16]. The simultaneous TG–DTA curves of stoichiometrically added precursor gels of samples A–E (before combustion) and as prepared powders (after combustion) are shown in the Fig. 4a–d. TG–DTA curves for pure zinc nitrate hexahydrate [$Zn(NO_3)_2{\cdot}6H_2O$], and pure glycine are given elsewhere [15], accordingly two-step mass loss was observed in pure glycine and zinc nitrate. Pure zinc nitrate decomposes completely below 330 °C. When pure glycine alone was subjected to DTA, one strong endothermic and two exothermic peaks were observed in the range 266–640 °C.

First strong endothermic peak in the range 206–290 °C indicates simultaneous melting and evolution of H_2O and NH_3 molecules. It is known that amino acids do not exhibit clean melting; they decompose into lower mass compounds.

Second exothermic peak in the range 290–410 °C indicates removal of water molecule formed as condensation product and NO_x. Third exothermic peak in the range 450–650 °C indicates removal of CO_2 molecules.

TG–DTA graphs (Fig. 4a, b) of gel precursors of samples A–C show two-step mass losses. First decomposition step associated with strong endothermic effects in the range room temperature to 110 °C corresponding to evaporation and volatilization of residual-free water. The second mass

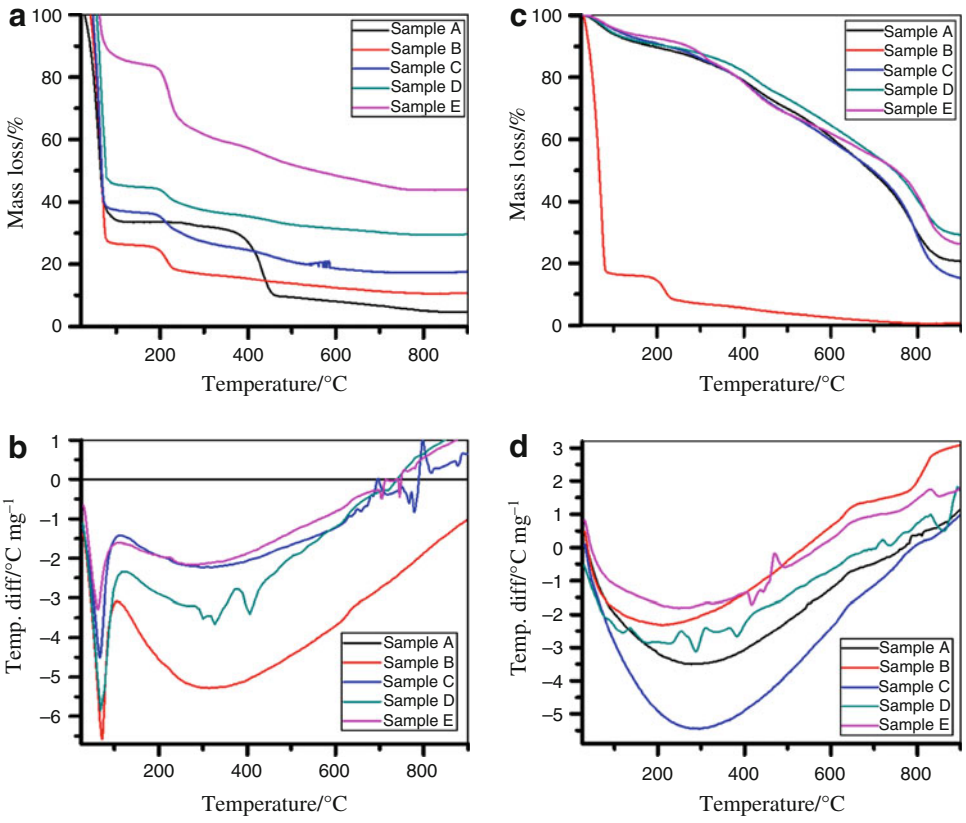

Fig. 4 TG–DTA curves of samples A–E, **a** TG curves of precursor gel, **b** DTA curves of precursor gel, **c** TG curves of as prepared powders, and **d** DTA curves of as prepared powders

loss observed in the region 325–485 °C for undoped ZnO (sample A), 120–620 °C for 0.1 and 0.5% Cu-doped ZnO (samples B and C) associated to endothermic peak corresponding to evolution of NO_3^-, along with oxidation of glycine by nitrate anions NO_3^- (resulting CO_2, $N_{2(g)}$, NO_2, and H_2O). Broadness of endothermic peak for 0.1 and 0.5% Cu-doped ZnO might be due to complexation reaction of Zn, Cu, and glycine as a ligand.

TG–DTA curves (Fig. 4a, b) of gel precursors of samples D and E show three-step mass loss. First mass loss is associated with intense endothermic peak in the region (room temperature to 110 °C), corresponds to evaporation and volatilization of residual-free water. Second mass loss corresponds to a broad endotherm which might be due to formation of aqua–hydroxo complex. While the third mass loss is gradual with small endothermic peaks in DTA graph, as structural rearrangements of lattice.

Samples A and C (Fig. 4c, d) as prepared powders show gradual mass loss, while sample B shows two-step mass losses in TG graph but DTA shows two distinct endothermic peaks. The peak from room temperature to 620 °C corresponds to evolution of water molecules and simultaneous evolution of NO_3^-, while second endotherm from 660 to 800 °C corresponds to desorption of carbonaceous matter.

TG–DTA curves (Fig. 4c, d) for as prepared samples D and E, which shows six-step decomposition in the temperature range of 30–850 °C. The total observed mass loss is 80%. The first two decomposition steps (room temperature to 130 °C and 135–260 °C) associated with endothermic effects correspond to evolution of residual water molecules. Further decomposition steps that are associated with small but narrow endothermic peaks correspond to intermediate formation of aqua–hydroxo complex of molecular formula $[ZnCu(H_2O)_x(OH)_y]O_{4-y}$. Similar phenomena have been explained by Carp et al. [35] in the thermal behavior of coordination complexes of copper ferrite with glycine. Formation of such aqua–hydroxo species may be explained as: during last decomposition steps highly reactive solid residue forms, which reacts with water generated during redox reaction of glycine with NO_3^-, this is also indicated by continuous weight loss in TG graph, also supported by FTIR spectra. The endothermicity of this process may be related to some structural rearrangements of the lattice and shows stable formation of Cu–ZnO after 850 °C. Similar work on decomposition of transition metal complexes to mixed and doped oxides were monitored by TG–DTA analysis by Mojumdar et al. [38–54].

Conclusions

We report successful synthesis of ZnO and various percentages (0.1–5%) of Cu–ZnO by aqueous thermolysis method using glycine as a fuel and capping agent. This study demonstrates the versatility of aqueous thermolysis method to yield monophasic Cu-doped ZnO. Doped and undoped ZnO have shown hexagonal phase and wurtzite symmetry. FTIR and thermal studies have confirmed intermediate formation of aqua–hydroxo complex which on further heating form Cu–ZnO. The endothermicity in TG–DTA graph is related to structural rearrangements of the lattice. ZnO nanoparticles have more novel quality than their bulk materials. Further studies on ZnO nanoparticles and thereby its influence on photocatalytic and humidity sensing performance of the material is underway in our laboratory.

Acknowledgements Mrs. Supriya N. Rishikeshi is thankful to Indian Space Research Organization (ISRO) for financial support and Dr. Prajakta Patil for her initial help in characterization of samples

References

1. Kryshtab TG, Khomchenko VS, Papusha VP, Mazin MO, Tzykunov YA. Thin ZnS:Cu, Ga and ZnO:Cu, Ga film phosphors. Thin Solid Films. 2002;403–404:76–80.
2. Navale SC, Ravi V, Srinivas D, Mulla IS, Gosavi SW, Kulkarni SK. EPR and DRS evidence for NO_2 sensing in Al-doped ZnO. Sens Actuators B. 2008;130:668–73.
3. Xiao Q, Zhang J, Xiao C, Tan X. Photocatalytic decolorization of methylene blue over $Zn_{1-x}Co_xO$ under visible light irradiation. Mater Sci Eng B. 2007;142:121–5.
4. Kutty TRN, Raghu N. Varistors based on polycrystalline ZnO:Cu Appl. Phys Lett. 1989;54:1796–8.
5. He L, Liu Y, Mustapha A, Lin M. Antifungal activity of zinc oxide nanoparticles against *Botrytis cinerea* and *Penicillium expansum*. Microbiol Res. 2011;166:207–15.
6. Carnes CL, Klabunde KJ. Synthesis, isolation, and chemical reactivity studies of nanocrystalline zinc oxide. Langmuir. 2000;16:3764–72.
7. Chang S, Sakai A. Luminescence properties of Zn nanowires prepared by electrochemical etching. Mater Lett. 2002;53:432–6.
8. Liu T, Sakurai O, Mizutani N, Kato M. Preparation of spherical fine ZnO particles by the spray pyrolysis method using ultrasonic atomization techniques. J Mater Sci. 1986;21:3698–702.
9. Shaoa ZB, Wanga CY, Genga SD, Suna XD, Geng SJ. Fabrication of nanometer-sized zinc oxide at low decomposing temperature. J Mater Process Technol. 2006;178:247–50.
10. Guo Y, Cao X, Lan X, Zhao C, Xue X, Song Y. Solution-based doping of manganese into colloidal ZnO nanorods. J Phys Chem C. 2008;112:8832–8.
11. Fernandes DM, Silva R, Winkler Hechenleitner AA, Radovanovic E, Custódio Melo MA, Gómez Pineda EA. Synthesis and characterization of ZnO, CuO and a mixed Zn and Cu oxide. Mater Chem Phys. 2009;115:110–5.
12. Yan B, Zhu H. Induced synthesis ZnO nanoparticles using novel amphiphilic zinc precursor complex with mono-octadecyl cis-butene dicarboxylate. J Optoelectron Adv Mater. 2007;9:3734–9.
13. Xiang L, Fei–Fei Z, Ying L, Sheng CM, Fu-Chi W, Xi-Xiang Z. Synthesis and photoluminescence study on ZnO nano-particles. Chin Phys Soc. 2007;16:2769–804.
14. Yadav BC, Srivastava R, Dwivedi CD, Pramanik P. Moisture sensor based on ZnO nanomaterial synthesized through oxalate route. Sens Actuators B. 2008;131:216–22.

15. Hwang CC, Wu TY. Combustion synthesis of nanocrystalline ZnO powders using zinc nitrate and glycine as reactants influence of reactant composition. J Mater Sci. 2004;39:6111–5.
16. Patil PR, Joshi SS. Polymerized organic–inorganic synthesis of nanocrystalline zinc oxide. Mater Chem Phys. 2007;105:354–61.
17. Patil PR, Joshi SS. Synthesis of a-Fe_2O_3 nanocubes. Synth React Inorg Met Org Nano-Met Chem. 2007;37:425–9.
18. Wu N, Zhao M, Zheng JG, Jiang C, Myers B, Li S, Chyu M, Mao SX. Porous CuO–ZnO nanocomposite for sensing electrode of high-temperature CO solid-state electrochemical sensor. Nanotechnology. 2005;16:2878–81.
19. Kanai Y. Jpn J Appl Phys. 1991;30:703.
20. Kalidindi S, Jagirdar BR. Synthesis of Cu@ZnO core–shell nanocomposite through digestive ripening of Cu and Zn nanoparticles. J Phys Chem C. 2008;112:4042–8.
21. Kim JB, Byun D, Ie SY, Park DH, Choi WK, Choi J, Angadi B. Cu-doped ZnO-based p–n hetero-junction light emitting diode. Semicond Sci Technol. 2008;23:095004–10.
22. Wang R, Lin H. Cu doped ZnO nanoparticle sheets. Mater Chem Phys. 2011;125:263–6.
23. Das K, Ray S, Chaudhari S, Maity AB. Structural and luminescence proprties of sol–gel derived Cu doped ZnO films. Ind J Pure Appl Phys. 2009;47:377–82.
24. Wang XB, Song C, Geng KW, Zeng F, Pan F. Photoluminescence and Raman scattering of Cu-doped ZnO films prepared by magnetron sputtering. Appl Surf Sci. 2007;253:6905–9.
25. Rai P, Tripathy S, Park N, Lee I, Yu Y. CTAB-assisted hydrothermal synthesis of single-crystalline copper-doped ZnO nanorods and investigation of their photoluminescence properties. J Mater Sci. 2010;. doi:10.1007/s10854-010-0055-5.
26. Zhang Z, Yi JB, Ding J, Wong LM, Seng HL, Wang SJ, Tao JG, Li GP, Xing GZ, Sum TC, Huan CHA, Wu T. Cu-doped ZnO nanoneedles and nanonails: morphological evolution and physical properties. J Phys Chem C. 2008;112:9579–85.
27. Freeman HC. Inorganic biochemistry, vol. 1. Amsterdam: Elsevier; 1973. p. 121.
28. Mojumdar S, Moresoli C, Simon L, Legge R. Edible wheat gluten (WG) protein films: preparation, thermal, mechanical and spectral properties. J Therm Anal Calorim. 2011;104:929–36.
29. Thakur P, Joshi SS, Kapoor S, Mukherjee T. Fluorescence behavior of cysteine-mediated Ag@CdS nanocolloids. Langmuir. 2009;25:6334–40.
30. Mimani T, Patil KC. Solution combustion synthesis of nanoscale oxides and their composites. Mater Phys Mech. 2001;4:134–7.
31. Chu D, Zeng YP, Jiang D. Hydrothermal synthesis and optical properties of Pb^{2+} doped ZnO nanorods. Mater Lett. 2006;60:2783–5.
32. Wolpert M, Hellwig P. Infrared spectra and molar absorption coefficients of the 20 alpha amino acids in aqueous solutions in the spectral range from 1800 to 500 cm^{-1}. Spectrochim Acta A. 2006;64:987–1001.
33. Barlow SM, Kitching KJ, Haq S, Richardson NV. A study of glycine adsorption on a Cu{110} surface using reflection absorption infrared spectroscopy. Surf Sci. 1998;401:322–35.
34. Coates J. Interpretation of infrared spectra: a practical approach. In: Meyer RA, editor. Encyclopedia of analytical chemistry. Chichester: Wiley; 2006.
35. Carp O, Gingasu D, Mindru I, Patron L. Thermal decomposition of some copper–iron polynuclear coordination compounds containing glycine as ligand, precursors of copper ferrite. Thermochim Acta. 2006;449:55–60.
36. Mokkelbost T, Kaus I, Greande T, Einarsrud M. Combustion synthesis and characterization of nanocrystalline CeO_2-based powders. Chem Mater. 2004;16:5489–94.
37. Mojumdar SC, Prasad R, Sun L, Venart JES, Eichhorn SH, Iqbal M, Elkamel A, Madhurambal G, Meenakshisundaram S, Varshney KG, Verenkar VMS, Jona E, Janotka I, Ray A, Chowdhury B. An introduction to thermodynamic modeling, thermal analysis and calorimetry. Res J Chem Environ. 2009;13(4):86–103.
38. Gawas UB, Verenkar VMS, Mojumdar SC. Synthesis and characterization of $Ni_{0.6}Zn_{0.4}Fe_2O_4$ nano-particles obtained by auto catalytic thermal decomposition of carboxylato-hydrazinate complex. J Therm Anal Calorim. 2011;104:879–83.
39. Gonsalves LR, Mojumdar SC, Verenkar VMS. Synthesis and characterisation of $Co_{0.8}Zn_{0.2}Fe_2O_4$ nanoparticles. J Therm Anal Calorim. 2011;104:869–73.
40. Gonsalves LR, Mojumdar SC, Verenkar VMS. Synthesis of cobalt nickel ferrite nanoparticles via autocatalytic decomposition of the precursor. J Therm Anal Calorim. 2010;100:789–92.
41. Gawas UB, Mojumdar SC, Verenkar VMS. Synthesis, characterization, infrared studies and thermal analysis of $Mn_{0.6}Zn_{0.4}Fe_2(C_4H_2O_4)_{3.6}N_2H_4$ and its decomposition product $Mn_{0.6}Zn_{0.4}Fe_2O_4$. J Therm Anal Calorim. 2010;100:867–71.
42. Gawas UB, Mojumdar SC, Verenkar VMS. $Ni_{0.5}Mn_{0.1}Zn_{0.4}$–$Fe_2(C_4H_2O_4)_{3.6}N_2H_4$ precursor and $Ni_{0.5}Mn_{0.1}Zn_{0.4}Fe_2O_4$ nanoparticle: preparation, IR spectral, XRD, SEM-EDS and thermal analysis. J Therm Anal Calorim. 2009;96:49–52.
43. Gonsalves LR, Verenkar VMS, Mojumdar SC. Preparation and characterization of $Co_{0.5}Zn_{0.5}Fe_2$ $(C_4H_2O_4)_{3.6}N_2H_4$: a precursor to prepare $Co_{0.5}Zn_{0.5}Fe_2O_4$ nanoparticles. J Therm Anal Calorim. 2009;96:53–7.
44. More A, Verenkar VMS, Mojumdar SC. Nickel ferrite nanoparticles synthesis from novel fumarato-hydrazinate precursor. J Therm Anal Calorim. 2008;94(1):63–7.
45. Madhurambal G, Ramasamy P, Anbusrinivasan P, Vasudevan G, Kavitha S, Mojumdar SC. Growth and characterization studies of 2-bromo-4-chloroacetophenone (BCAP) crystals. J Therm Anal Calorim. 2008;94:59–62.
46. Mojumdar SC, Sain M, Prasad R, Sun L, Venart JES. Thermoanalytical techniques and their applications from medicine to construction Part I. J Therm Anal Calorim. 2007;90(3):653–62.
47. Mojumdar SC, Capek I, Capek P, Fialová L, Berek D. Preparation of composite nanoparticles on the base of starch. Res J Chem Environ. 2007;11:5–12.
48. Sawant SY, Verenkar VMS, Mojumdar SC. Preparation, thermal, XRD, chemical and FTIR spectral analysis of $NiMn_2O_4$ nanoparticles and respective precursor. J Therm Anal Calorim. 2007;90:669–72.
49. Mojumdar SC, Raki L. Synthesis, thermal and structural characterization of nanocomposites for potential application in construction. J Therm Anal Calorim. 2006;86:651–7.
50. Porob RA, Khan SZ, Mojumdar SC, Verenkar VMS, Synthesis TG. DSC and infra-red study of $NiMn_2(C_4H_4O_4)_{3.6}N_2H_4$, a precursor for $NiMn_2O_4$ nanoparticles. J Therm Anal Calorim. 2006;86:605–8.
51. Dová M, Palou M, Mojumdar SC. Hydration behavior of C_2S and C_2As nanomaterials, synthesized by sol–gel method. J Therm Anal Calorim. 2006;86:595–9.
52. Mojumdar SC, Raki L. Preparation, thermal, spectral and microscopic studies of calcium silicate hydrate-poly(acrylic acid) nanocomposite materials. J Therm Anal Calorim. 2006;85:99–105.
53. Mojumdar SC, Raki L, Mathis N, Schimdt K, Lang S. Synthesis, thermal conductivity, TG/DTA, AFM, FTIR, ^{29}Si and ^{13}C NMR studies of calcium silicate hydrate–polymer nanocomposite materials. J Therm Anal Calorim. 2006;85:119–24.
54. Mojumdar SC, Raki L. Preparation and properties of calcium silicate hydrate-poly(vinyl alcohol) nanocomposite materials. J Therm Anal Calorim. 2005;82:89–95.